Isomer-Selective Study of the OH-Initiated Oxidation of Isoprene in the Presence of O-2 and NO: 2. The Major OH Addition Channel

ARTICLE *in* THE JOURNAL OF PHYSICAL CHEMISTRY A · FEBRUARY 2010

Impact Factor: 2.69 · DOI: 10.1021/jp909052t · Source: PubMed

Isomer-Selective Study of the OH-Initiated Oxidation of Isoprene in the Presence of O_2 and NO: 2. The Major OH Addition Channel

Buddhadeb Ghosh, Alejandro Bugarin, Brian T. Connell, and Simon W. North*

Department of Chemistry, Texas A&M University, P.O. Box 30012, College Station, Texas 77842

Received: September 18, 2009; Revised Manuscript Received: January 6, 2010

We report the first isomeric-selective study of the dominant isomeric pathway in the OH-initiated oxidation of isoprene in the presence of O_2 and NO using the laser photolysis−laser induced fluorescence (LP−LIF) technique. The photolysis of monodeuterated/nondeuterated 2-iodo-2-methylbut-3-en-1-ol results exclusively in the dominant OH−isoprene addition product, providing important insight into the oxidation mechanism. On the basis of kinetic analysis of OH cycling experiments, we have determined the rate constant for O_2 addition to the hydroxyalkyl radical to be $1.0^{+1.7}_{-0.5} \times 10^{-12}$ cm^3 s^{-1}, and we find a value of $8.1^{+3.4}_{-2.3} \times 10^{-12}$ cm^3 s^{-1} for the overall reaction rate constant of the resulting hydroxyperoxy radical with NO. We also report the first clear experimental evidence of the (*E*) form of the δ-hydroxyalkoxy channel through isotopic labeling experiments and quantify its branching ratio to be (10 ± 3)%. This puts a rigorous upper limit on the branching of the (*E*)-δ-hydroxyalkoxy radical channel. Since our measured isomeric-selective rate constants for the dominant outer channel in OH-initiated isoprene chemistry are similar to the overall rate constants derived from nonisomeric kinetics, we predict that the remaining outer addition channel will have similar reactivity.

I. Introduction

Isoprene (2-methyl-1,3-butadiene) is the dominant non-methane organic compound (NMOC) emitted into the atmosphere by vegetation with an annual global emission rate of ~500 Tg.[1] It represents almost 50% of all biogenic non-methane hydrocarbons on a global scale,[2] with an atmospheric concentration between 1−30 ppb.[3,4] In the atmosphere, isoprene reacts with the OH radical, NO_3 radical, Cl radical, and O_3,[5] although a strong diurnal emission rate and high reactivity toward the OH radical results in chemistry dominated by OH-initiated oxidation (90%) with an atmospheric lifetime with respect to the OH radical of approximately 1.5 h.[6] The OH-initiated oxidation of isoprene is a central issue in atmospheric chemistry and is responsible for 50−100% of ozone production attributed to VOC oxidation in the continental U.S.,[4] which has adverse effect on vegetation[7,8] and human health.[7] Isoprene oxidation also leads to the formation of organic nitrates, which are responsible for removal of as much as 7% of the NO emitted in North America in the summer time,[6] accounting for 4% of nitrogen oxide transported from North America.[9] Isoprene is responsible for a 10% increase in the half-life of methane.[10] Finally, the oxidation of isoprene leads to US and global biogenic SOA formation of 50% and 58%, respectively.[11,12,13]

The addition of OH to isoprene results in four distinct hydroxyl alkyl isomers (Figure 1), each of which ultimately leads to different first-generation end products. Although there has been no direct experimental determination of the branching between channels, theoretical work has predicted branching of 0.67, 0.02, 0.02, and 0.29, respectively, for isomers I, II, III, and IV,[14] with an overall rate of $(1.0 \pm 0.1) \times 10^{-10}$ molecule^{-1} cm^3 s^{-1}.[14–19] End product analysis studies also suggest that OH addition occurs preferentially at the terminal carbons.[20,21]

The radicals formed from OH addition to the terminal carbons react with molecular oxygen under atmospheric conditions to form peroxy radicals, which subsequently react with NO to form alkoxy radicals. This contrasts with the dominant pathway for the radicals formed from OH addition to the inner carbons. For these radicals, recent studies have demonstrated that prompt isomerization to form α-hydroxyl alkyl radicals occurs followed by reaction with oxygen to form C_5 carbonyl compounds and HO_2.[22–24]

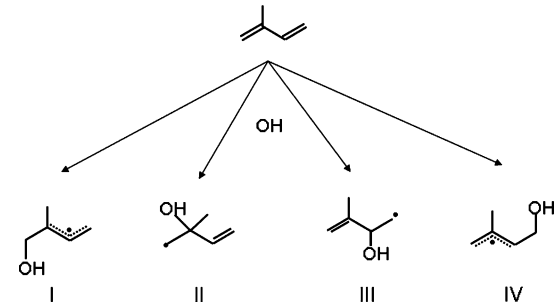

Figure 1. Initial branching of hydroxyalkyl radicals followed by the reaction of OH radical with isoprene.

Theoretical studies suggest that decomposition is the sole fate for the β-hydroxyalkoxy radicals[25–27] leading to the formation of methylvinyl ketone, methacrolein, and formaldehyde as first-generation end products.[28–34] The δ-hydroxyalkoxy radicals however, undergo prompt 1,5 hydrogen shift[35,36] followed by hydrogen abstraction or reaction with O_2 to form C_5 or C_4 hydroxycarbonyl compounds.[37] Hydrogen abstraction by O_2 during the oxidation process generates HO_2, which reacts with NO to regenerate OH radicals. Thus, the time-dependent kinetics of OH in the presence of NO and O_2 is a sensitive probe of the detailed mechanism of the oxidation process.

Until recently, studies of isoprene chemistry have been non-isomer-specific, that is, they reflect the reactivity of the combined pathways and are often insensitive to specific details of the isomeric pathways. In a previous study, we demonstrated that isomer-selective kinetic experiments permit the investigation of minor important channels in isoprene oxidation that are

* To whom correspondence should be addressed.

10.1021/jp909052t
Published on Web 02/01/2010

obscured by the major channel kinetics.[22,23] The photodissociation of a suitable iodohydrin precursor provides a route to the formation of a single OH−isoprene adduct isomer, enabling such studies. In the present study, we focus on the major channel of the isoprene oxidation, and to this end, we have synthesized the photolytic precursor 2-iodo-2-methylbut-3-en-1-ol. In doing so, we reduce the complex chemistry of isoprene oxidation to the chemistry of a single pathway (species I in Figure 1), permitting determination of isomer-specific kinetic rate constants.

Product studies on the isoprene oxidation account for only 60−70% of the carbon balance (MVK + formaldehyde ≈ 30%; MACR + formaldehyde ≈ 27%; organic nitrate ≈ 10%; furan derivative ≈ 3%),[32] while predicting that carbonyl compounds may account for the remaining 30%.[34] Theory suggests that the major channel for isoprene oxidation may lead to ∼20% of the carbonyl compounds through δ-hydroxyalkoxy radicals.[37] Isomeric-selective studies would be valuable in assessing the chemistry that gives rise to the production of hydroxy carbonyls. The δ-hydroxyalkoxy radical can exist in either the (*E*) or the (*Z*) form. The yield of the (*E*)-δ-hydroxyalkoxy channel, although predicted from theoretical calculations,[32,35] has yet to be measured experimentally since the complexity of the reaction systems has precluded a direct experimental confirmation. Isomer-selective isotopically labeled OH cycling experiments may provide quantification of this channel by measuring the relative formation of OD (*Z*) to OH formation (*E*).

The accuracy of regional air quality modeling depends on a detailed understanding of the mechanism of OH-initiated isoprene oxidation. The goal of our current study is to elucidate the mechanism of the dominant isomeric pathway of OH−isoprene oxidation and consequently assess the validity of condensed chemical oxidation models.

II. Experimental Section

The photolytic precursor, 2-iodo-2-methylbut-3-en-1-ol, was synthesized following the methodology reported by Snider et al.,[38] and we only provide a brief summary. Isoprene reacted with silver oxide (Ag_2O) and iodine (I_2) in molar ratio of 2:1:1 in 1:1 water (H_2O) and acetonitrile (MeCN)

$$\text{isoprene} \xrightarrow[\text{2.5 hrs, 25 C}]{\substack{Ag_2O/I_2 \\ MeCN/H_2O}} \text{primary alcohol} + \text{tertiary alcohol}$$

resulting in a 3:1 mixture of the tertiary and primary alcohol, respectively. The products were separated by solvent extraction and column chromatography and were identified by NMR, mass spectrometry, and IR spectroscopy (provided in the Supporting Information).

A detailed description of LP/LIF experiment has been given elsewhere,[39,40] and here, we present only the salient features. The 248 nm beam from an EX10 Excimer laser (GAM laser) was used to photolyze the 2-iodo-2-methylbut-3-en-1-ol or the monodeuterated variant. The excimer beam was collinearly aligned through the kinetic cell with the probe laser beam tuned to 282 or 287 nm, used for the LIF detection of OH or OD, respectively. The probe beam was generated by doubling the output from a dye laser (Quantel TDL-51) running Rhodamine 590 dye or a mixture of Rhodamine 590 and Rhodamine 610 dye pumped by a 532 nm beam from an Nd:YAG laser (Spectra Physics Quanta Ray INDI). The OH/OD radical concentrations were monitored by measuring the OH/OD fluorescence by exciting at the Q_1 (1) transition of the A ← X (1, 0) band. The resulting fluorescence was collected by a lens assembly and passed through an optical filter where it was detected by a photomultiplier tube (PMT) and integrated by a using a digital oscilloscope. The time delay between the two lasers was controlled by a digital delay generator (SRS DG-535). The 2-iodo-2-methylbut-3-en-1-ol precursor was introduced into the reaction cell using an MKS flow meter by flowing argon through a bubbler that contained the sample at room temperature (vapor pressure ≈ 1.5 Torr). NO (Sigma Aldrich, 98.5%) was purified to remove HONO and NO_2 by using an ascarite trap before buffering it with argon in a 5 L bulb and was introduced into the chamber through an MKS flow meter. The NO concentration inside of the cell was varied from 8.2×10^{14} to 3.9×10^{15} molecules cm^{-3}, and the O_2 concentration was varied from 7.8×10^{15} to 6.20×10^{16} molecules cm^{-3}. The temperature of the reaction cell was maintained at room temperature (297 ± 3 K), and an MKS baratron was used to monitor the total pressure inside of the cell, which was buffered to 50 ± 1 Torr with argon.

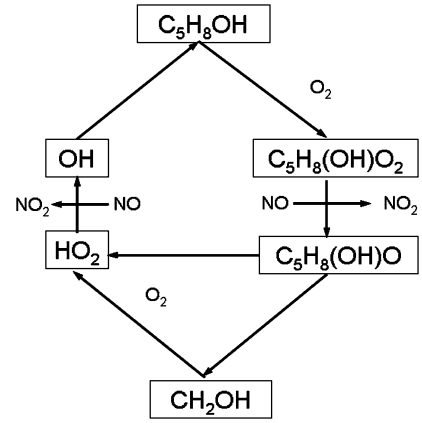

Figure 2. Schematic diagram of OH cycling in isoprene oxidation.

III. Results and Discussion

In this section, we present the results obtained from OH cycling experiments and the related analysis of the data. We first describe OH cycling experiments using a nondeuterated precursor molecule, including a discussion on sensitivity analysis of the derived rate constants. Next, we describe kinetic experiments using a deuterated precursor molecule and the determination of branching between β- and δ-hydroxyalkoxy radicals.

A. OH Cycling from the Nondeuterated Precursor. In these experiments, the precursor molecule, 2-iodo-2-methylbut-3-en-1-ol, was dissociated by a 248 nm laser pulse to form the radical (I) of the four possible isomers of hydroxyl isoprene radical (Figure 1). A simplified mechanism of OH cycling is described schematically in Figure 2. The kinetics experiments rely on the time-dependent formation of OH as a function of O_2 and NO concentrations to provide information about rate constants of intermediate reactions and can be effective with judicious choice of experimental conditions guided by sensitivity analysis. These experiments were performed in a moderate to high NO concentration to ensure OH cycling, and the O_2 concentrations were maintained at a higher value to ensure a higher rate of OH formation than loss (see text below). A summary of the concentrations of reacting species is tabulated in Table 1 below.

Figure 3 shows a typical set of experimental data from OH cycling experiments where the concentration of the precursor molecule was 2.1×10^{13} molecules cm^{-3}, the concentration of NO was 2.8×10^{15} molecules cm^{-3}, and the O_2 concentrations were varied from 7.8×10^{15} to 1.5×10^{16} molecules cm^{-3}.

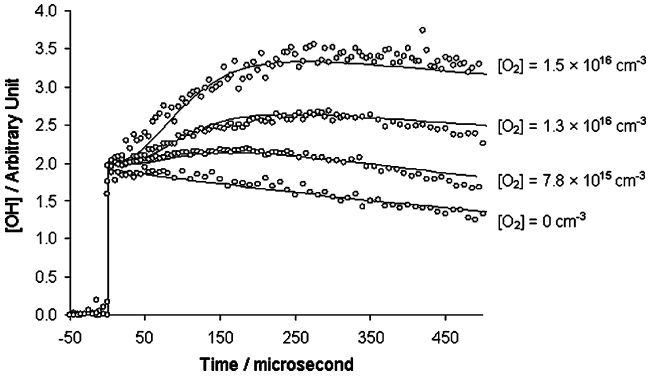

Figure 3. OH fluorescence intensity plotted against the reaction time at multiple O_2 concentrations. The symbols represent experimental data, and the solid lines represent the fits using the reaction mechanism and rate constants in Table 3. $[IC_5H_8OH] = 2.1 \times 10^{13}$ molecules cm^{-3}; $[NO] = 2.8 \times 10^{15}$ molecules cm^{-3}. The last plot was taken in the absence of O_2.

TABLE 1: Summary of the Experimental Conditions Applied in This Study

[precursor] 10^{13} molecules/cc	[NO] 10^{14} molecules/cc	[O_2] 10^{15} molecules/cc
OH Cycling Experiments from IC_5H_8OH		
2.1	28.0	7.8
2.1	28.0	13.0
2.1	28.0	15.0
3.8	6.1	9.8
3.8	8.0	9.8
1.5	9.7	40.2
1.5	13.8	26.2
OH Cycling Experiments from IC_5H_8OD		
1.4	28.0	29.4
1.4	28.0	31.4
1.4	28.0	36.0
1.4	28.0	60.0
OD Cycling Experiments from IC_5H_8OD		
1.4	35.0	54.0
1.4	35.0	75.0

The prompt rise in OH signal following precursor photolysis is due to the fraction (25−30%) of nascent hydroxyl alkyl radicals produced with energy exceeding the threshold to decomposition to form OH and isoprene prior to collisional stabilization. In the absence of O_2 and NO, this OH signal exhibits an exponential decay due to reaction with the precursor with a rate constant of $k_{23} = 1.3 \times 10^{-11}$ molecules^{-1} cm^3 s^{-1}. This value is similar to values measured for the rate of OH addition to similar compounds,[22,23] presumably via OH addition to the iodohydrin double bond. In the presence of O_2 and NO, photolysis of the iodohydrin precursor and subsequent chemistry results in a OH signal that exhibits an initial rise over 150−300 μs due to the cycling mechanism shown in Figure 2 followed by decay due to termination reactions.

The numerical program KINTECUS[41] was used to simulate the experimental data as well as to perform sensitivity analysis. The 25 reactions that were used to simulate the OH cycling data are provided in Table 3 along with the corresponding rate constants. A more detailed 30 reaction mechanism which includes the OH cycling arising from the reaction of the OH radical with the precursor molecule IC_5H_8OH is given in the Supporting Information (Table T1). The fits using the extended model are virtually indistinguishable from those using the concise model as the OH cycling from the precursor molecule has little effect in the current experimental conditions. Therefore, we have used a simpler and more concise model in the paper to fit our data. The best fits to the data are shown as the solid lines in Figure 3. The reaction mechanism given in Table 3 is shown in Figure 4. One of the goals of the current study is to determine the rate constants for the intermediate reactions based on time-dependent hydroxyl radical measurements as a function of O_2 and NO concentrations. In order to assess the viability of extracting intermediate rate constants in this way, we rely on sensitivity analysis, which describes the dependence of the data on specific rate constants in the reaction mechanism.[42] The normalized sensitivity coefficient (NSC) is defined as

$$\mathrm{NSC} = \left[\frac{\delta \ln[\mathrm{OH}]}{\delta \ln k_i}\right]_{j \neq i}$$

where k_i represents the rate constant of the ith reaction in the reaction mechanism and [OH] represents the concentration of the hydroxyl radical at a specific time. A NSC of 1.0, for example, indicates that a 20% change in the rate constant i results in a 20% change in the OH concentration at a given time.

Figure 5 shows NSCs for all of the rate constants in the reaction mechanism evaluated at a NO concentration of 2.8×10^{15} molecules cm^{-3} and two different O_2 concentrations of 1.5×10^{16} and 7.9×10^{15} molecules cm^{-3}, respectively, at a reaction time of 171 μs. It is clear from inspection of Figure 5 that the OH concentration profile depends sensitively on a limited number of rate constants, specifically, the branching between metastable hydroxyalkyl radicals which decompose and thermalized hydroxyalkyl radicals (k_1 and k_2), the rate constant for the reaction of NO and hydroxyalkyl radical (k_3), the reaction of O_2 and hydroxyalkyl radicals (k_4), and the reaction of NO and the hydroxyalkylperoxy radical (k_7). Although the NSC for the NO + HO_2 rate constant (k_{24}) is comparable with that of the peroxy radical reaction with NO, it is a well-studied reaction, and we have adopted the reported room-temperature values.[16,43]

At moderate to high NO concentrations, the radical chain termination steps arising from the addition of NO to radical

TABLE 2: Summary of End Product Distributions (in percentage yield) Predicted by the Branching Ratios Determined in This Study[a]

end product OH−isoprene adduct ratio	current study I/II/III/IV 67:2:2:29		current study I/II/III/IV 56:2.3:4.6:37		MIM2[61]	Zhao[34]	Jenkin[62]	Atkinson[28]
nitrate yield	5.0	15.0	5.0	15.0	10.0		10.0	12.0
MVK	50.9	45.6	42.5	38.1	45.6	55.0	33.1	29.0
MACR	22.0	19.8	28.1	25.2	22.1		22.2	21.0
OH carbonyl	18.0	15.5	17.4	15.1	22.3	22.6	20.2	25.0

[a] Included are the end product distributions used in several other chemical models.

TABLE 3: Kinetics Mechanism Employed in Modeling the Time-Dependent OH Signals[a]

	reaction	rate constant	ref	comment
k_1	$HOC_5H_8 \rightarrow OH + C_5H_8$	prompt (30%)	*b*	
k_2	$HOC_5H_8 \rightarrow HOC_5H_8$	prompt (70%)	*b*	
k_3	$HOC_5H_8 + NO \rightarrow HOC_5H_8NO$	1.2×10^{-11}	*b*	
k_4	$HOC_5H_8 + O_2 \rightarrow \beta$-$HOC_5H_8O_2$	8.0×10^{-13}	*b*	β- branching
k_5	$HOC_5H_8 + O_2 \rightarrow Z$-$HOC_5H_8O_2$	1.0×10^{-13}	*b*	Z-δ branching
k_6	$HOC_5H_8 + O_2 \rightarrow E$-$HOC_5H_8O_2$	1.0×10^{-13}	*b*	E-δ branching
k_7	β-$HOC_5H_8O_2 + NO \rightarrow \beta$-$HOC_5H_8O + NO_2$	7.0×10^{-12}	*b*	
k_8	β-$HOC_5H_8O_2 + NO \rightarrow \beta$-$HOC_5H_8ONO_2$	1.1×10^{-12}	53, 54	
k_9	Z-$HOC_5H_8O_2 + NO \rightarrow Z$-$OHC_5H_7OH + NO_2$	7.0×10^{-12}	*b*	
k_{10}	Z-$HOC_5H_8O_2 + NO \rightarrow Z$-$HOC_5H_8ONO_2$	1.1×10^{-12}	53, 54	peroxy radicals reacting with
k_{11}	E-$HOC_5H_8O_2 + NO \rightarrow E$-$OHC_5H_7OH + NO_2$	7.0×10^{-12}	*b*	NO to form alkoxy radicals
k_{12}	E-$HOC_5H_8O_2 + NO \rightarrow E$-$HOC_5H_8ONO_2$	1.1×10^{-12}	53, 54	
k_{13}	β-$HOC_5H_8O \rightarrow CH_2OH + OC_4H_6$	prompt	25–27	
k_{14}	Z-$OHC_5H_7OH + O_2 \rightarrow HO_2 + OC_5H_7OH$	1.0×10^{-11}	16	chemistry of Z-δ channel
k_{15}	Z-$OHC_5H_7OH + NO \rightarrow Z$-$OHC_5H_7OHNO$	3.0×10^{-11}	44, 45, 47, 48	
k_{16}	E-$OHC_5H_7OH + NO \rightarrow E$-$OHC_5H_7OHNO$	1.2×10^{-11}	*b*	
k_{17}	E-$OHC_5H_7OH + O_2 \rightarrow E$-$OHC_5H_7OHO_2$	1.0×10^{-12}	*b*,35	
k_{18}	E-$OHC_5H_7OHO_2 + NO \rightarrow E$-$OHC_5H_7OHO + NO_2$	7.0×10^{-12}	*b*,35	chemistry of E-δ channel
k_{19}	E-$OHC_5H_7OHO_2 + NO \rightarrow E$-$OHC_5H_7OHONO_2$	1.1×10^{-12}	53, 54	
k_{20}	E-$OHC_5H_7OHO \rightarrow OHC_4H_5O + CH_2OH$	prompt	44	
k_{21}	$CH_2OH + O_2 \rightarrow CH_2O + HO_2$	1.0×10^{-11}	16	
k_{22}	$CH_2OH + NO \rightarrow CH_2OHNO$	1.2×10^{-11}	19	
k_{23}	$OH + IHOC_5H_8 \rightarrow IHOC_5H_8OH$	1.3×10^{-11}	*b*	
k_{24}	$HO_2 + NO \rightarrow OH + NO_2$	8.8×10^{-12}	43	
k_{25}	$OH + NO \rightarrow HONO$	9.4×10^{-13}	63, 64	

[a] Rate constants are in molecule^{-1} cm^3 s^{-1} unless otherwise stated. [b] This work.

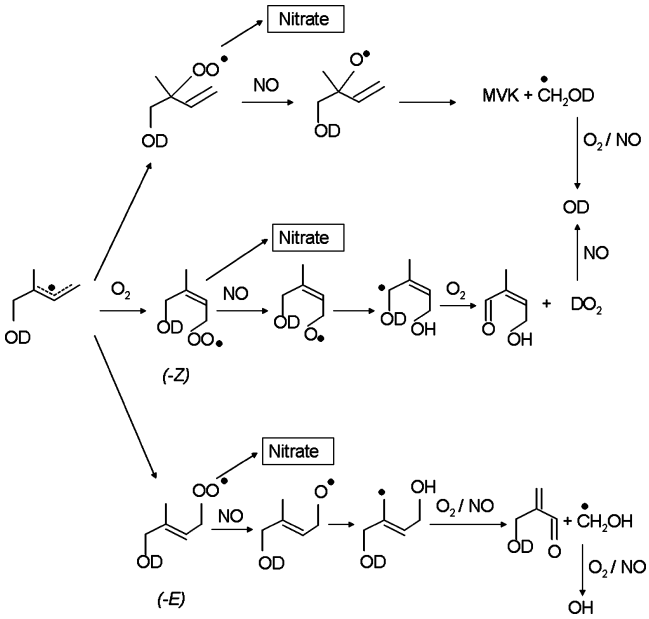

Figure 4. Oxidation mechanism of isomer I.

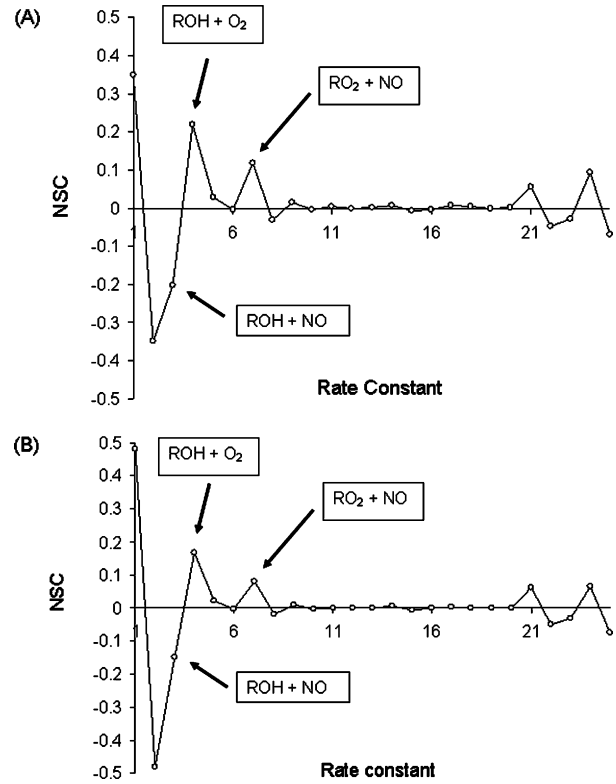

Figure 5. (A) Sensitivity analysis at time 171 μs for $[IC_5H_8OH] = 2.1 \times 10^{13}$ molecules cm^{-3}, $[NO] = 2.8 \times 10^{15}$ molecules cm^{-3}, and $[O_2] = 1.5 \times 10^{16}$ molecules cm^{-3}. (B) Sensitivity analysis at time 170 μs for $[IC_5H_8OH] = 2.1 \times 10^{13}$ molecules cm^{-3}, $[NO] = 2.8 \times 10^{15}$ molecules cm^{-3}, and $[O_2] = 7.9 \times 10^{15}$ molecules cm^{-3}.

species become important as it affects the overall decay of the signal. The mechanism needs to incorporate these steps since the NO concentrations employed in this study are relatively high to ensure rapid cycling. We have used a rate constant of $k_{15} = 3.0 \times 10^{-11}$ cm^3 molecule^{-1} s^{-1}, for the reaction of hydroxyalkoxy radical and NO, which is based on the value reported by Park et al.,[44] and the recommendation made by Atkinson for similar reactions.[45] It is also similar to the rate constant of $3.9 \pm 0.3 \times 10^{-11}$ cm^3 molecule^{-1} s^{-1} reported by Lotz and Zellner for the reaction of the 2-butoxyl radical with NO.[46] Work by Deng et al.[47] and Blitz et al.[48] also supports adopting a pressure-independent rate constant of 3.0×10^{-11} cm^3 molecule^{-1} s^{-1} for this reaction. The NO addition to CH_2OH has been assigned a rate of $k_{22} = 1.2 \times 10^{-11}$ cm^3 molecule^{-1} s^{-1} based on recommendations from other studies.[19]

At moderate to high concentrations of O_2, sensitivity analysis predicts a moderate NSC for the rate constant of O_2 addition to the hydroxyalkyl radical. We have calculated the dependence of the NSC for $(k_4 + k_5 + k_6)$ as a function of time delay and O_2 concentration. The NSC reaches a maximum value for O_2 concentrations near 1.5×10^{16} molecules cm^{-3}. As a result,

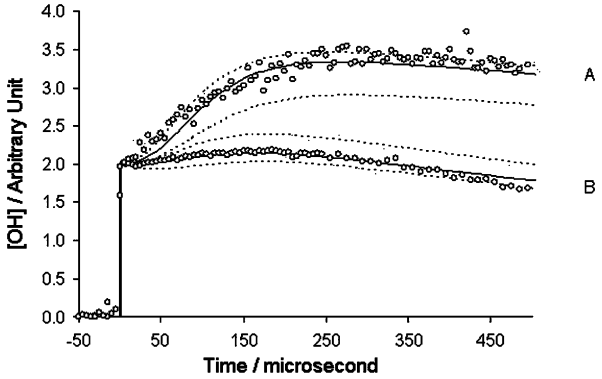

Figure 6. Dashed lines indicate the rate constants for the estimated error range for O_2 addition to hydroxyalkyl radical ($k4 + k_5 + k_6$). (A) $[IC_5H_8OH] = 2.1 \times 10^{13}$ molecules cm^{-3}, $[NO] = 2.8 \times 10^{15}$ molecules cm^{-3}, and $[O_2] = 1.5 \times 10^{16}$ molecules cm^{-3}. Upper limit $= 2.7 \times 10^{-12}$ molecule^{-1} cm^3 s^{-1}; lower limit $= 5.0 \times 10^{-13}$ molecule^{-1} cm^3 s^{-1}. (B) $[IC_5H_8OH] = 2.1 \times 10^{13}$ molecules cm^{-3}, $[NO] = 2.8 \times 10^{15}$ molecules cm^{-3}, and $[O_2] = 7.8 \times 10^{15}$ molecules cm^{-3}. Upper limit $= 2.7 \times 10^{-12}$ molecule^{-1} cm^3 s^{-1}; lower limit $= 5.0 \times 10^{-13}$ molecule^{-1} cm^3 s^{-1}.

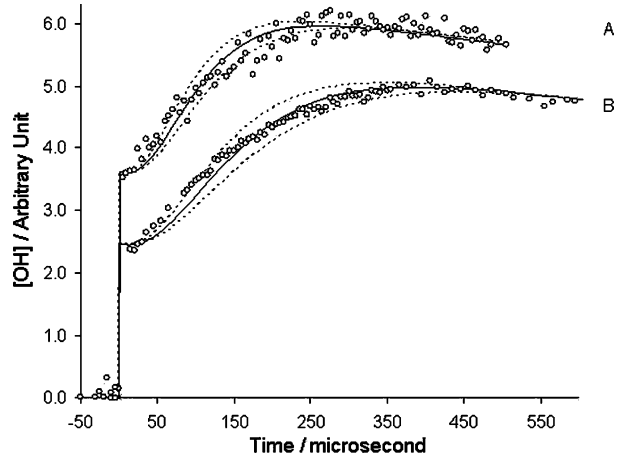

Figure 7. Dashed lines indicate the rate constants for the estimated error range for the NO reaction with hydroxyalkylperoxy radical rate ($k_7 + k_8$). (A) $[IC_5H_8OH] = 2.1 \times 10^{13}$ molecules cm^{-3}, $[NO] = 2.8 \times 10^{15}$ molecules cm^{-3}, and $[O_2] = 1.5 \times 10^{16}$ molecules cm^{-3}. Upper limit $= 11.5 \times 10^{-12}$ molecule^{-1} cm^3 s^{-1}; lower limit $= 5.8 \times 10^{-12}$ molecule^{-1} cm^3 s^{-1}. (B) $[IC_5H_8OH] = 2.5 \times 10^{13}$ molecules cm^{-3}, $[NO] = 1.7 \times 10^{15}$ molecules cm^{-3}, and $[O_2] = 2.3 \times 10^{16}$ molecules cm^{-3}. Upper limit $= 11.5 \times 10^{-12}$ molecule^{-1} cm^3 s^{-1}; lower limit $= 5.8 \times 10^{-12}$ molecule^{-1} cm^3 s^{-1}.

we have employed similar oxygen concentrations in our experiments to ensure maximum sensitivity to this rate constant in our simulations.

The addition of either O_2 or NO to the hydroxyalkyl radical represents a competition between radical chain propagation ($k_4 + k_5 + k_6$) and chain termination (k_3), and it is the relative magnitude of these two rates, that is, k_3[NO] and $(k_4 + k_5 + k_6)[O_2]$, that controls the shape of the simulated curve. As a consequence, both rate constants are strongly coupled. Thus, the value of k_3 will have an effect on the value of ($k_4 + k_5 + k_6$), and the range of k_3 will help to determine the range for ($k_4 + k_5 + k_6$). However, according to previous studies, the value of the NO addition rate constant has a relatively narrow range,[22,23,44] and we have adopted values ranging from 7.0×10^{-12} to 2.0×10^{-11} molecule^{-1} cm^3 s^{-1} (Figure S1, Supporting Information). We were unable to achieve satisfactory fits to our experimental data with values for k_3 outside of this range. We chose a value of 1.2×10^{-11} molecule^{-1} cm^3 s^{-1} for k_3 since this value provides the best fit to the experimental data and agrees well with values used in previous studies.[23,44] Using this fixed value of 1.2×10^{-11} molecule^{-1} cm^3 s^{-1} for the rate of the hydroxy radical reaction with NO (k_3), we find the best fit for the O_2 addition rate to the hydroxy radical of 1.0×10^{-12} molecule^{-1} cm^3 s^{-1}, with an upper limit of 1.8×10^{-12} molecule^{-1} cm^3 s^{-1} and a lower limit of 6.0×10^{-13} molecule^{-1} cm^3 s^{-1}. When we include the range of k_3, the error bars on ($k_4 + k_5 + k_6$) reflect the interdependence of these rate constants. For this range of the NO addition rate constant (k_3), we find the upper and lower limits of the O_2 addition rate change to be 2.7×10^{-12} and 5.0×10^{-13} molecule^{-1} cm^3 s^{-1}, respectively (Figure 6). Thus, the uncertainty in the value of k_3 results in a higher uncertainty in the value of ($k_4 + k_5 + k_6$), and we report a value of $1.0^{+1.7}_{-0.5} \times 10^{-12}$ cm^3 s^{-1} for the O_2 addition to the hydroxyalkyl radical.

Although the exact value of this rate constant is unimportant under atmospheric conditions due to the high O_2 concentration, the value is necessary for accurate modeling of laboratory kinetics studies. Rate constants for O_2 addition to the hydroxyalkyl radical have been calculated theoretically, and the rate constant for isomer I was reported to be 2.7×10^{-12} molecule^{-1} cm^3 s^{-1} [49] in the range of our observed value. The rate constant that we determined lies within the range of $(7.0 \pm 3.0) \times 10^{-13}$ molecule^{-1} cm^3 s^{-1} determined from non-isomer-selective experimental studies performed by Zhang et al.[50] It is also within the range of 6.0×10^{-13}–2.0×10^{-12} molecule^{-1} cm^3 s^{-1} determined by Koch et al.[51] at 345 and 300 K and is consistent with the range of $(2.3 \pm 2.0) \times 10^{-12}$ molecule^{-1} cm^3 s^{-1} determined by Park et al.,[44] both based on non-isomer-selective cycling experiments. The rate agrees with the rates on the order of 10^{-12} molecule^{-1} cm^3 s^{-1} reported by Atkinson[45] for alkyl radicals.

The hydroxyperoxy radical reacts with NO under atmospheric conditions to form an activated nitrite species which promptly decomposes to form a hydroxyalkoxy radical and NO_2, with a minor fraction isomerizing to form the stable nitrate.[52] Previous laboratory measurements of the rate constant for the hydroxyperoxy radical + NO reaction involved direct monitoring of the reactant hydroxyperoxy radical, that is, measurement of the overall loss rate via the pseudo-first-order decay of the hydroxyperoxy radical.[53,54] In the present study, sensitivity analysis predicts a moderate NSC for NO to NO_2 conversion but a small NSC for the minor nitrate formation reaction. Thus, we are sensitive only to the rate constant k_7 and, on the basis of previous reports, have adopted a nitrate yield of 15% to assign a value for k_8.[53,54] The 15% nitrate yield represents the higher end of the predicted nitrate yield,[37,44] which ranges from 4 to 15%. We have calculated the NSC for the hydroxyalkylperoxy radical + NO rate constant as a function of both reaction time and O_2 concentration. The sensitivity of the data to the rate constant increases with time to a maximum value near the observed onset of cycling (180 μs). The NSC also increases with increasing concentration of oxygen, reflecting the higher formation rate for the hydroxyalkylperoxy radical. We find that the NSC levels off at higher O_2 concentrations since the yield of the hydroxyalkylperoxy radical becomes invariant. On the basis of such analysis, we have determined a rate constant for the overall reaction of NO with the hydroxylalkylperoxy radical of $8.1^{+3.4}_{-2.3} \times 10^{-12}$ molecule^{-1} cm^3 s^{-1}, which agrees with other reported values.[45] Figure 7 shows the best fit (solid line) to the data obtained by using the above-mentioned value for the NO reaction rate with the hydroxylalkylperoxy radical, and the dashed lines represent upper and lower error bounds of 11.5 ×

10^{-12} and 5.8×10^{-12} molecule^{-1} cm^3 s^{-1} respectively. The value for this rate constant lies in the range of $(9.0 \pm 3.0) \times 10^{-12}$ molecule^{-1} cm^3 s^{-1}, reported by the cycling[44] study by Park et al. and the value determined from direct measurement[54] of the rate constant by Zhang et al. This value is also in good agreement with the overall rate constant of $(8.8 \pm 1.2) \times 10^{-12}$ molecule^{-1} cm^3 s^{-1} reported for this reaction by Miller et al.[53] and is close to the value of 7.6×10^{-12} molecule^{-1} cm^3 s^{-1} recommended by Paulson et al. for atmospheric modeling.[32]

Unimolecular reactions in the oxidation mechanism that arise from activated, nonthermal species have rate constants that exceed or are comparable to the collision frequency and are treated as instantaneous on the time scale of the overall kinetics. We have denoted these reactions (k_{13} and k_{20}) as prompt in Table 3, and the simulations are insensitive to the value utilized, provided the rate constants are $>1.0 \times 10^6$ s^{-1}. The absolute values for these rate constants were not determinable in the current study, and we have used recommended rates from previous studies.[44]

The reaction rate constants k_4, k_5, and k_6 in Table 3 correspond to relative branching ratios of different peroxy radicals. Reaction 4 corresponds to the branching ratio of β-hydroxyperoxy radicals, which subsequently react with NO to form β-hydroxyalkoxy radicals that undergo prompt decomposition. Reaction 5 corresponds to the branching of the *Z*-δ-hydroxyperoxy radicals which reacts with NO to form the corresponding alkoxy radicals, and reaction 6 refers to the branching ratio of the *E*-δ-hydroxyalkoxy radicals which reacts with NO to form its corresponding alkoxy radical. The *E* and *Z* forms of the δ-hydroxyalkoxy radicals undergo one to five hydrogen shifts to form dihydroxy radicals (Figure 4). The *Z* form of the dihydroxy radical reacts with molecular oxygen by a H-abstraction mechanism to form a C_5-hydroxycarbonyl, whereas the *E* form of the dihydroxy radical reacts with O_2 and NO and subsequently decomposes to form a C_4-hydroxycarbonyl.[25] Dibble has reported another potential pathway for the (*E*)-OHC_5H_7OH isomer from theoretical studies, which leads to the formation of a C_5-dihydroxycarbonyl compound.[25] However, no product study has observed this species,[29] and we have concluded that the yield of this channel would be negligible;[55] hence we have not included this channel in our model. Dibble has also reported another potential fate of the *Z*-δ-hydroxyalkylalkoxy radical when it reacts with another oxygen molecule following electron delocalization.[56] However, the same author also suggests that the fractional yield of the above-mentioned channel would be very small (1−2%);[56] hence, we have not included this chemistry in our model. We find that an 80:20 relative branching between the β- and δ-peroxy radicals provides the best fit to all of the data. Since theoretical calculations predict equivalent branching between the *E* and *Z* forms due to the low barrier associated with *E*/*Z* isomerization compared to the initial activation energy,[35] a 20% branching for δ-peroxy radicals corresponds to a branching of 10% for both *E* and *Z* channels. Our sensitivity analyses conclude that the current experiment is only moderately sensitive to the branching between the β- and the δ-hydroxyalkoxy radical channels and motivate our study of isotopically labeled OH/OD cycling.

B. Isotopically Labeled OH/OD Cycling Experiments. The use of a precursor molecule where OH has been replaced by OD can provide additional insight into the role of the *E*-δ-hydroxyalkoxy radical. As illustrated in Figure 4, in an isotopically labeled experiment, both the β-hydroxyalkoxy radical channel and the *Z* form of the δ-hydroxyalkoxy radical channel lead to the formation of OD. In contrast, the *E* form of the δ-hydroxyalkoxy radical will lead to the formation of OH. Thus, the observation of OH formation from a deuterated precursor is a signature of the production of the *E* form of the δ-hydroxyalkoxy radical channel. To pursue these studies, the precursor molecule was deuterated by dissolution in D_2O for 30 min, followed by extraction from the aqueous solution. The reaction cell was passivated with D_2O to reduce H/D exchange from the hydrogen adsorbed in the kinetic cell and inlet lines. Figure 8 shows the OH signal observed from cycling experiments using the photolysis of the deuterated precursor. This observation provides the first direct evidence for the role of the (*E*)-δ-hydroxyalkoxy channel in isoprene oxidation. The lower signal-to-noise ratio in this data is consistent with the low branching ratio (0.1) for this channel. It is clear from the data shown in Figure 8 that there appears to be a small contribution from prompt OH formation even though a purely deuterated precursor should only give rise to prompt OD signal. This suggests that there is a small fraction of deuterated precursor that undergoes H/D exchange prior to photolysis despite efforts to minimize exchange. The photolysis of this nondeuterated precursor should result in a similar fraction (25−30%) of prompt OH and isoprene prior to collisional stabilization. The dashed line shown in Figure 8 is a simulation assuming no exchange in the mechanism, while the solid line is a simulation assuming that only 6% of the deuterated precursor molecule undergoes H/D exchange prior to photolysis. This small contribution from H/D exchange provides a better fit to the experimental data. A significant fraction of H/D exchange would result in a much larger prompt signal, which is not observed. Although including the minor contribution of H/D exchange in the model improves the fit, the experimental results are still consistent with the presence of the (*E*)-δ-hydroxyalkoxy channel.

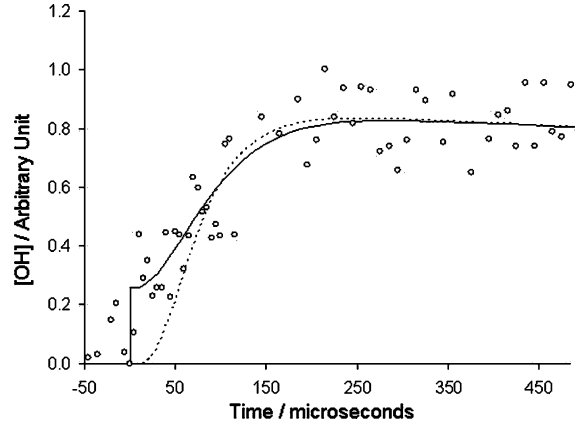

Figure 8. OH cycling from a deuterated precursor. $[IC_5H_8OD] = 1.4 \times 10^{13}$ molecules cm^{-3}, $[NO] = 2.8 \times 10^{15}$ molecules cm^{-3}, and $[O_2] = 3.3 \times 10^{16}$ molecules cm^{-3}. The dashed line assumes no H/D exchange, while the solid line assumes 6% H/D exchange (see text for details).

Figure 9 shows the OD signal obtained from the OD cycling experiments using the deuterated precursor. In OD cycling using a deuterated precursor, a clear prompt rise in signal is seen, followed by a gradual change of signal over time similar to the data shown in the nondeuterated studies in Figure 3. Since the (*E*)-δ-hydroxyalkoxy channel results in OH from a deuterated precursor, this channel decreases the amount of OD production due to cycling relative to the prompt OD signal. In this data, it is therefore the decrease in the ratio of the cycling signal to the prompt rise which provides an additional constraint in quantifying the yield of the (*E*)-δ-hydroxyalkoxy channel. The best fit to this data, as shown by the solid line, corresponds to a (*E*)-δ-hydroxyalkoxy channel branching of 10%, whereas the dashed

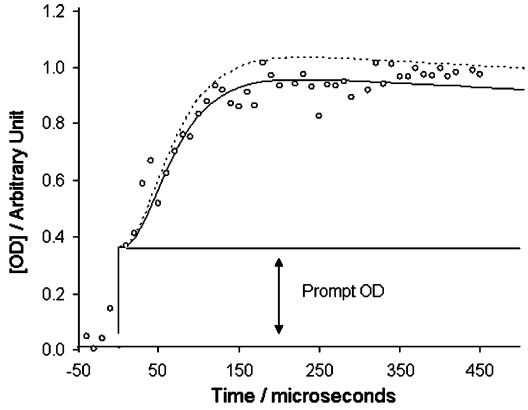

Figure 9. OD cycling from the deuterated precursor. $[IC_5H_8OD] = 1.4 \times 10^{13}$ molecules cm^{-3}, $[NO] = 3.5 \times 10^{15}$ molecules cm^{-3}, and $[O_2] = 5.4 \times 10^{16}$ molecules cm^{-3}. The solid line assumes a branching of 0.2 for the δ-hydroxyalkoxy channel, while the dashed line assumes a branching of 0.0 for the δ-hydroxyalkoxy channel (see text for details).

line corresponds to no δ-hydroxyalkoxy channel (Figure 9). It is worth noting here that alternate chemistry reported by Paulot and co-workers[57] suggests that the (*Z*)-δ-dihydroxy radical may also undergo a second O_2 addition, as opposed to undergoing H abstraction, to form a dihydroxyperoxy radical, which undergoes further reactions to finally form HO_2, a route to produce OH via the (*Z*)-δ-dihydroxy radical channel starting from a deuterated precursor, in contrast to our model. The authors reported a branching of 0.35 for this dihydroxyperoxy channel within the *(Z)*-δ-peroxy channel and a branching of 0.65 for the traditional (*Z*)-δ-dihydroxy radical chemistry where the radical reacts with oxygen via hydrogen abstraction to form a hydroxycarbonyl and thus not leading to OH formation from a deuterated precursor. However, a fraction of the *Z*-dihydroxyperoxy radical channel, which leads to methylglyoxal and glycolaldehyde, will lead to the formation of OD from a deuterated precursor, and hence, this model with these reported branching ratios will result in only half of the OH signal from a deuterated precursor compared to what is observed in our isotopically labeled experiments. The branching of 0.35 for the O_2 addition channel seems to be an overestimate as previous studies suggest that α-hydroxy radicals react with O_2 almost exclusively by H abstraction.[58–60] The authors have also suggested that the *E*/*Z* branching would not be 1:1 but rather 0.15/0.85. Also, previous computational work[35] and modeling studies[32,37] have estimated a nearly equivalent branching for the *E* and the *Z* isomers of δ-hydroxyperoxy radical channels. Furthermore, the chemistry proposed by Paulot et al.[57] predicts formation of 3−4% of methylglyoxal and glycolaldehyde as first-generation end products, which is contradictory to previous end product analysis studies.[28,61] Thus, although this chemistry will reproduce our experimental results, we have not included this chemistry in our model as we think it will have a small contribution. A χ^2 analysis of the simulation fit to the data indicates that the error in this branching ratio is ±3%, resulting in a final branching for the *E* channel of (10 ± 3)%, which will provide an upper limit to the branching of the (*E*)-δ-peroxy channel in case any other chemistry is capable of producing OH from a deuterated precursor. Assuming an equal yield of the *E* and the *Z* isomers of δ-hydroxyperoxy radical channels, this corresponds to a yield of (20.0 ± 5.0)% for the δ-hydroxyalkoxy channel, consistent with our nonisotopic results but with better error limits.

IV. Predicted End Product Distribution

This study has determined a branching ratio of (10 ± 3)% for the *E* form of the δ-hydroxyalkoxy radical channel and predicts an overall (20 ± 6)% yield for the δ-hydroxyalkoxy radical. Since the rate constants obtained in this study of the major channel are very similar to those obtained for isoprene−OH oxidation as a whole,[44] we predict that the other terminal OH addition channel (channel IV in Figure 1) will exhibit similar chemistry. On the basis of this assumption, we have predicted the end product distribution for two different initial hydroxyalkyl radical branching of 0.67:0.02:0.02:0.29[14] and 0.56:0.023:0.046:0.37[15] for the channel I/II/III/IV and assuming two limiting values for the nitrate yields of 5 and 15%. The results are shown in Table 2.

The yields of MVK, MACR, and hydroxycarbonyls vary from 38 to 51%, from 20 to 28%, and from 15 to 18%, respectively. These predicted yields are close to those found in other studies and used in chemical models. The predicted MVK yields probably represent the upper limit, but it depends largely on the initial branching of hydroxyalkyl radicals I, II, III, and IV (Figure 1). We did not measure that branching in this study, and we have used reported value from literature. There are other conflicting values in the literature for that initial branching, and they lead to different final product yields. The hydroxycarbonyl yield from the current study is within the margin of error of other studies but is lower. Our current results for the terminal OH addition to isoprene, coupled with previous studies on the OH addition to inner carbons of isoprene,[22] enable us to express the OH-initiated oxidation of isoprene under high NO_x conditions using a condensed mechanism (assuming an initial branching of I/II/III/IV = 67:2:2:29) of isoprene + OH = $0.10RONO_2 + 0.90HO_2 + 0.48MVK + 0.21MACR + 0.21ISPD + 0.92NO_2 + 0.75HCHO$, where $RONO_2$ = organic nitrate (assuming 10% nitrate yield), ISPD = first-generation products other than MVK, MACR: hydroxycarbonyls, and C_5-carbonyls, and NO_2 = total NO_2 formed from NO.

V. Conclusions

The current study is the first isomeric-selective study on the major channel of isoprene oxidation. The results of the OH cycling experiment provide insight into channel branching and yield isomeric-selective rate constants. Sensitivity analysis has been employed to ensure that experimental conditions are suitable for determination of the rate constant for O_2 addition to the hydroxyalkyl radical and for NO reaction with the hydroxyperoxy radicals, and we have determined the rate constants of $1.0^{+1.7}_{-0.5} \times 10^{-12}$ and $8.1^{+3.4}_{-2.3} \times 10^{-12}$ molecule^{-1} cm^3 s^{-1}, respectively. Isotopically labeled studies have provided the first experimental evidence of the δ-hydroxyalkoxy channel, and we have determined an upper limit of (10 ± 3)% on the branching of the *E* form of the δ-hydroxyalkoxy radical channel. Since the values of the intermediate rate constants for this major channel are similar to the values obtained for isoprene as a whole, we surmise that the other major channel (isomer IV in Figure 1) must have similar kinetic parameters associated with the OH-initiated oxidation. Hence, a condensed model including the chemistry of the δ-peroxy channel should provide an accurate enough description of isoprene−OH chemistry at high NO_x conditions.

Acknowledgment. This work was supported by the Environmental Protection Agency (EPA), the Texas Commission on Environmental Quality (TCEQ), and the Robert A. Welch Foundation (A-1405). The authors gratefully acknowledge the

experimental assistance provided by Trevor Makal and Dr. Kristin S. Dooley.

Supporting Information Available: Additional results. This material is available free of charge via the Internet at http://pubs.acs.org.

References and Notes

(1) Chameides, W. L.; Fehsenfeld, F.; Rodgers, M. O.; Cardelino, C.; Martinez, J.; Parrish, D.; Lonneman, W.; Lawson, D. R.; Rasmussen, R. A.; Zimmerman, P.; Greenberg, J.; Middleton, P.; Wang, T. *J. Geophys. Res.* **1992**, *97*, 6037.

(2) Guenther, A.; Hewitt, C. N.; Erickson, D.; Fall, R.; Geron, C.; Graedel, T.; Harley, P.; Klinger, L.; Lerdau, M.; McKay, W. A.; Pierce, T.; Scholes, B.; Steinbrecher, R.; Tallamraju, R.; Taylor, J.; Zimmerman, P. *J. Geophys. Res.* **1995**, *100*, 8873.

(3) Martin, R. S.; Westberg, H.; Allwine, E.; Ashman, L.; Farmer, J. C.; Lamb, B. *J. Atmos. Chem.* **1991**, *13*, 1.

(4) Wiedinmyer, C.; Friedfeld, S.; Baugh, W.; Greenberg, J.; Guenther, A.; Fraser, M.; Allen, D. *Atmos. Environ.* **2001**, *35*, 1001.

(5) Poschl, U.; von Kuhlmann, R.; Poisson, N.; Crutzen, P. J. *J. Atmos. Chem.* **2000**, *37*, 29.

(6) Chen, X. H.; Hulbert, D.; Shepson, P. B. *J. Geophys. Res.* **1998**, *103*, 25563.

(7) Engardt, M. *J. Atmos. Chem.* **2008**, *59*, 61.

(8) Wang, D.; Bormann, F. H.; Karnosky, D. F. *Environ. Sci. Technol.* **1986**, *20*, 1122.

(9) Horowitz, L. W.; Liang, J. Y.; Gardner, G. M.; Jacob, D. J. *J. Geophys. Res.* **1998**, *103*, 13451.

(10) Sasaki, K.; Saito, T.; Lämsä, M.; Oksman-Caldentey, K. M.; Suzuki, M.; Ohyama, K.; Muranaka, T.; Ohara, K.; Yazaki, K. *Plant Cell Physiol.* **2007**, *48*.

(11) Claeys, M.; Graham, B.; Vas, G.; Wang, W.; Vermeylen, R.; Pashynska, V.; Cafmeyer, J.; Guyon, P.; Andreae, M. O.; Artaxo, P.; Maenhaut, W. *Science* **2004**, *303*, 1173.

(12) Kroll, J. H.; Ng, N. L.; Murphy, S. M.; Flagan, R. C.; Seinfeld, J. H. *Geophys. Res. Lett.* **2005**, 32.

(13) Liao, H.; Henze, D. K.; Seinfeld, J. H.; Wu, S. L.; Mickley, L. J. *J. Geophys. Res.* **2007**, 112.

(14) Greenwald, E. E.; North, S. W.; Georgievskii, Y.; Klippenstein, S. J. *J. Phys. Chem. A* **2007**, *111*, 5582.

(15) Lei, W. F.; Zhang, R. Y.; McGivern, W. S.; Derecskei-Kovacs, A.; North, S. W. *Chem. Phys. Lett.* **2000**, *326*, 109.

(16) Atkinson, R.; Baulch, D. L.; Cox, R. A.; Crowley, J. N.; Hampson, R. F., Jr.; Kerr, J. A.; Rossi, M. J.; Troe, J. *Summary of Evaluated Kinetic and Photochemical Data for Atmospheric Chemistry. IUPAC Subcommittee on Gas Kinetic Data Evaluation for Atmospheric Chemistry*; Blackwell: London 2002.

(17) Chuong, B.; Stevens, P. S. *J. Phys. Chem. A* **2000**, *104*, 5230.

(18) Kleindienst, T. E.; Harris, G. W.; Pitts, J. N. *Environ. Sci. Technol.* **1982**, *16*, 844.

(19) Pagsberg, P.; Munk, J.; Anastasi, C.; Simpson, V. J. *J. Phys. Chem.* **1989**, *93*, 5162.

(20) Jenkin, M. E.; Hayman, G. D. *Journal of the Chemical Society-Faraday Transactions* **1995**, *91*, 1911.

(21) Tuazon, E. C.; Atkinson, R. *Int. J. Chem. Kinet.* **1989**, *21*, 1141.

(22) Greenwald, E. E.; Ghosh, B.; Anderson, K. C.; Dooley, K.; Zou, P.; Selby, T.; Osborn, D. L.; Meloni, G.; Taatjes, C. A.; Leone, S. R.; North, S. W. *J. Phys. Chem. A* **2010**, *114*, 904.

(23) Greenwald, E. E.; Park, J.; Anderson, K. C.; Kim, H.; Reich, B. J. E.; Miller, S. A.; Zhang, R. Y.; North, S. W. *J. Phys. Chem. A* **2005**, *109*, 7915.

(24) Park, J.; Jongsma, C. G.; Zhang, R. Y.; North, S. W. *Phys. Chem. Chem. Phys.* **2003**, *5*, 3638.

(25) Dibble, T. S. *J. Phys. Chem. A* **1999**, *103*, 8559.

(26) Lei, W. F.; Zhang, R. Y. *J. Phys. Chem. A* **2001**, *105*, 3808.

(27) Park, J.; Stephens, J. C.; Zhang, R. Y.; North, S. W. *J. Phys. Chem. A* **2003**, *107*, 6408.

(28) Atkinson, R.; Aschmann, S. M.; Tuazon, E. C.; Arey, J.; Zielinska, B. *Int. J. Chem. Kinet.* **1989**, *21*, 593.

(29) Kwok, E. S. C.; Atkinson, R.; Arey, J. *Environ. Sci. Technol.* **1995**, *29*, 2467.

(30) Lloyd, A. C.; Atkinson, R.; Lurmann, F. W.; Nitta, B. *Atmos. Environ.* **1983**, *17*, 1931.

(31) Paulson, S. E.; Flagan, R. C.; Seinfeld, J. H. *Int. J. Chem. Kinet.* **1992**, *24*, 79.

(32) Paulson, S. E.; Seinfeld, J. H. *J. Geophys. Res.* **1992**, *97*, 20703.

(33) Tuazon, E. C.; Atkinson, R. *Int. J. Chem. Kinet.* **1990**, *22*, 1221.

(34) Zhao, J.; Zhang, R. Y.; Fortner, E. C.; North, S. W. *J. Am. Chem. Soc.* **2004**, *126*, 2686.

(35) Dibble, T. S. *J. Phys. Chem. A* **2002**, *106*, 6643.

(36) Zhao, J.; Zhang, R. Y.; North, S. W. *Chem. Phys. Lett.* **2003**, *369*, 204.

(37) Fan, J.; Zhang, R. *Environ. Chem.* **2004**, *1*, 140.

(38) Snider, B. B.; Duvall, J. R. *Tetrahedron Lett.* **2003**, *44*, 3067.

(39) McGivern, W. S.; Suh, I.; Clinkenbeard, A. D.; Zhang, R. Y.; North, S. W. *J. Phys. Chem. A* **2000**, *104*, 6609.

(40) Reitz, J. E.; McGivern, W. S.; Church, M. C.; Wilson, M. D.; North, S. W. *Int. J. Chem. Kinet.* **2002**, *34*, 255.

(41) Ianni, James C. A Comparison of the Bader-Deuflhard and the Cash-Karp Runge-Kutta Integrators for the GRI-MECH 3.0 Model Based on the Chemical Kinetics Code Kintecus, In *Computational Fluid and Solid Mechanics*; Bathe, K. J., Ed.; Elsevier Science Ltd.: Oxford, UK., 2003, pp 1368−1372.

(42) Steinfeld, J. I.; Francisco, J. S.; Hase, W. L. *Chemical Kinetics and Dynamics*; Prentice Hall International: Englewood Cliffs, NJ, 1989.

(43) DeMore, W. B.; Sander, S. P.; Golden, D. M.; Hampson, R. F.; Kurylo, M. J.; Howard, C. J.; Ravishankara, A. R.; Kolb, C. E.; Molina, M. J. *Chemical Kinetics and Photochemical Data for Use in Stratospheric Modeling*, JPL Publ. 09-25; Jet Propulsion Lab: Pasadena, CA, 2003.

(44) Park, J.; Jongsma, C. G.; Zhang, R. Y.; North, S. W. *J. Phys. Chem. A* **2004**, *108*, 10688.

(45) Atkinson, R. *J. Phys. Chem. Ref. Data* **1997**, *26*, 215.

(46) Lotz, C.; Zellner, R. *Phys. Chem. Chem. Phys.* **2001**, *3*, 2607.

(47) Deng, W.; Wang, C. J.; Katz, D. R.; Gawinski, G. R.; Davis, A. J.; Dibble, T. S. *Chem. Phys. Lett.* **2000**, *330*, 541.

(48) Blitz, M.; Pilling, M. J.; Robertson, S. H.; Seakins, P. W. *Phys. Chem. Chem. Phys.* **1999**, *1*, 73.

(49) Lei, W. F.; Zhang, R. Y.; McGivern, W. S.; Derecskei-Kovacs, A.; North, S. W. *J. Phys. Chem. A* **2001**, *105*, 471.

(50) Zhang, D.; Zhang, R. Y.; Church, C.; North, S. W. *Chem. Phys. Lett.* **2001**, *343*, 49.

(51) Koch, R.; Siese, M.; Fittschen, C.; Zetzsch, C. In a contribution to the *EUROTRAC subproject LACTOZ*; Fraunhofer Publica: Germany, 1995; p 268.

(52) Zhang, D.; Zhang, R. Y.; Park, J.; North, S. W. *J. Am. Chem. Soc.* **2002**, *124*, 9600.

(53) Miller, A. M.; Yeung, L. Y.; Kiep, A. C.; Elrod, M. J. *Phys. Chem. Chem. Phys.* **2004**, *6*, 3402.

(54) Zhang, D.; Zhang, R.; North, S. W. *J. Phys. Chem. A* **2003**, *107*, 11013.

(55) Carter, W. P. L.; Atkinson, R. *Int. J. Chem. Kinet.* **1996**, *28*, 497.

(56) Dibble, T. S. *J. Phys. Chem. A* **2004**, *108*, 2199.

(57) Paulot, F.; Crounse, J. D.; Kjaergaard, H. G.; Kroll, J. H.; Seinfeld, J. H.; Wenberg, P. O. *Atmos. Chem. Phys.* **2009**, *9*, 1479.

(58) Carter, W. P. L.; Darnall, K. R.; Graham, R. A.; Winer, A. M.; Pitts, J. N., Jr. *J. Phys. Chem.* **1979**, *83*, 2305.

(59) Washida, N. *J. Chem. Phys.* **1981**, *75*, 2715.

(60) Ohta, T.; Bandow, H.; Akimoto, H. *Int. J. Chem. Kinet.* **1982**, *14*, 173.

(61) Taraborrelli, D.; Lawrence, M. G.; Butler, T. M.; Sander, R.; Lelieveld, J. *Atmos. Chem. Phys.* **2009**, *9*, 2751.

(62) Jenkin, M. E.; Boyd, A. A.; Lesclaux, R. *J. Atmos. Chem.* **1998**, *29*, 267.

(63) Forster, R.; Frost, M.; Fulle, D.; Hamann, H. F.; Hippler, H.; Schlepegrell, A.; Troe, J. *J. Chem. Phys.* **1995**, *103*, 2949.

(64) Sander, S. P.; Friedl, R. R.; Golden, D. M.; Kurylo, M. J.; Moortgat, G. K. ; Wine, P. H.; Ravishankara, A. R.; Kolb, C. E.; Molina, M. J.; Finlayson-Pitts, B. J.; Huie, R. E.; Orkin, V. L. *Chemical Kinetics and Photochemical Data for Use in Stratospheric Modeling*, JPL Publ. 06-2; Jet Propulsion Lab: Pasadena, CA, 2006.

JP909052T